

Article

A Simple and Economical System for Automatic Near-Field Scanning for Power Electronics Converters

Sebastiano Grasso ¹, Salvatore Bellinvia ¹, Nunzio Salerno ²  and Santi Agatino Rizzo ^{2,*} 

¹ STMicroelectronics, Stradale Primosole 50, 95121 Catania, Italy; sebastiano-l1.grasso@st.com (S.G.); bellinvias91@gmail.com (S.B.)

² Department of Electrical Electronic and Computer Engineering (DIEE), University of Catania, 95125 Catania, Italy; nunzio.salerno@unict.it

* Correspondence: santi.rizzo@unict.it

Abstract: Electromagnetic compatibility issues must be considered from the early steps in the design of electronic devices. A specific topic is the near-field emission generated by the device due to the traces on a printed circuit board and the specific routing. The analysis of near-field emission is essential to detect potential electromagnetic interference with nearby devices. This problem is crucial in high power density applications. Therefore, especially in these applications, it is necessary to optimize the circuit and the layout to minimize the generated noise. The design and construction of systems able to scan volumes to determine the spatial distribution of electrical E and/or magnetic B fields in the near-field region of a device under test is a very complex process. The realization of equipment that explores a given surface at a given distance from the device is easier. The main purpose of this paper is to show how it is possible to build a cheap two-dimensional scanner, starting from simple hardware not explicitly designed for near-field scan operations. The presented firmware and software solution can map, with good accuracy, the spatial distribution of fields B and E on a fixed plan close to the board. Finally, the developed system has been used in a GaN-based bi-directional DC/DC Converter.

Keywords: electromagnetic compatibility; near-field scan; power electronics



Citation: Grasso, S.; Bellinvia, S.; Salerno, N.; Rizzo, S.A. A Simple and Economical System for Automatic Near-Field Scanning for Power Electronics Converters. *Energies* **2023**, *16*, 7868. <https://doi.org/10.3390/en16237868>

Academic Editor: Hervé Morel

Received: 9 October 2023

Revised: 20 November 2023

Accepted: 27 November 2023

Published: 1 December 2023



Copyright: © 2023 by the authors. Licensee MDPI, Basel, Switzerland. This article is an open access article distributed under the terms and conditions of the Creative Commons Attribution (CC BY) license (<https://creativecommons.org/licenses/by/4.0/>).

1. Introduction

Electromagnetic compatibility (EMC) today is vital and strategic, considering the growing complexity of any electronic device and the diffusion of electronic modules in every area of human life [1]. Before being put on the market, each electronic device must be tested to be certified as electromagnetically compatible [2]. There are two different aspects to be considered: the first one is the electromagnetic pollution generated in the environment by the equipment under testing (EUT) and the second one is the effects of external electromagnetic fields [3]. Moreover, some are related to electromagnetic pollution through the supply cables or the connections of the EUT and the load or its immunity to conducted noises through those connections. Others are related to electromagnetic pollution spread in the surrounding environment or to the sensibility of the EUT to the external radiated noise [3,4]. There are a lot of characterizations that could be performed to study these effects using electromagnetic simulation flows [5,6] or through mathematical models that are able to predict electromagnetic interference (EMI) phenomena [7,8]. In some cases, an electromagnetic evaluation is performed through a classical measurement approach on a prototype [9].

A specific EMC aspect of the study is the near-field emission generated by EUT [10] due to traces on a printed circuit board (PCB) and the particular routing. The analysis of near-field emission is essential to detect potential electromagnetic interference with nearby devices [11]. This problem is crucial in automotive and, in general, high power density applications. Additionally, it is possible to foresee the far-field emissions, and it could also

be possible to optimize the circuit and the layout to minimize the generated noise [12], starting from the near-field estimation.

Near-field emissions generated by EUT can be acquired using commercial equipment that provides accurate measurements and, in some cases, can be used for pre-compliant measurements. However, commercial equipment has a very high cost that ranges from some tens to one hundred thousand dollars. This is due to the complexity of designing and constructing systems that are able to scan volumes to determine the spatial distribution of electrical and/or magnetic fields in the near-field region of the EUT.

When the scanner is used for a rough analysis of electromagnetic emissions produced by a board and/or its use is sporadic, the investment in such expensive equipment cannot be justified. Therefore, in these cases, it is impossible to perform any electromagnetic measurements that could be useful for a first estimation of the board emission. In such circumstances, the realization of equipment that explores a given surface at a given distance from the device or the board under testing is useful.

From this perspective, the main purpose of this paper is to show how it is possible to build a homemade two-dimensional scanner that is able to map the spatial distribution of fields B and E on a fixed plan. For this purpose, the scanner has been obtained starting from simple hardware not specifically designed for near-field scan operations, whose bill of materials is less than two thousand dollars. This strong cost reduction compared to commercial tools is obtained thanks to the customization of the proposed system to the specific application. Hence, the customization has enabled the realization of a simpler and more economical scanner than the commercial ones, whose high complexity and cost are due to the many functionalities and tasks they are designed to perform.

The proposed approach has practical use in near-field scanning in the context of power electronics because it enables everyone to roughly estimate electromagnetic emissions by adopting solutions like the one proposed in this paper. These kinds of simple and economic systems can be used for tuning electromagnetic simulation parameters in order to validate finite element analysis that, in turn, can be used to optimize circuit layouts by estimating the electromagnetic emissions of different layouts before the prototyping stage.

The paper is organized as follows. In Section 2, the near-field scan equipment is described in detail; in Section 3, it is applied to a bi-directional DC/DC converter; and finally, conclusions are provided in Section 4.

2. Near-Field Scan Equipment

An electromagnetic near-field scan is a measurement process to determine the spatial distribution of electrical and/or magnetic fields in the near-field region of a device under test or on a board. Those fields are sensed through specific antennas, which convert the strength of the field into a voltage available at the 50 Ω port of those sensing elements. In the simplest systems, the spatial distribution is on a surface; in the most complicated ones, it is on a specific volume (Figure 1).

Generally, the voltage as a function of time or frequency is measured. It should be highlighted that the DUT may be considered as any object radiating or storing electromagnetic field energy intentionally or unintentionally. The voltage pattern is usually mapped on planar, cylindrical or spherical geometrical surfaces as a collection of a finite number of spatial samples.

These samples are usually converted into a color intensity map that lets it easily understand in which zone, on a volume or surface, the electromagnetic field generated by a specific source (a device or one or more parts of a board) is concentrated.

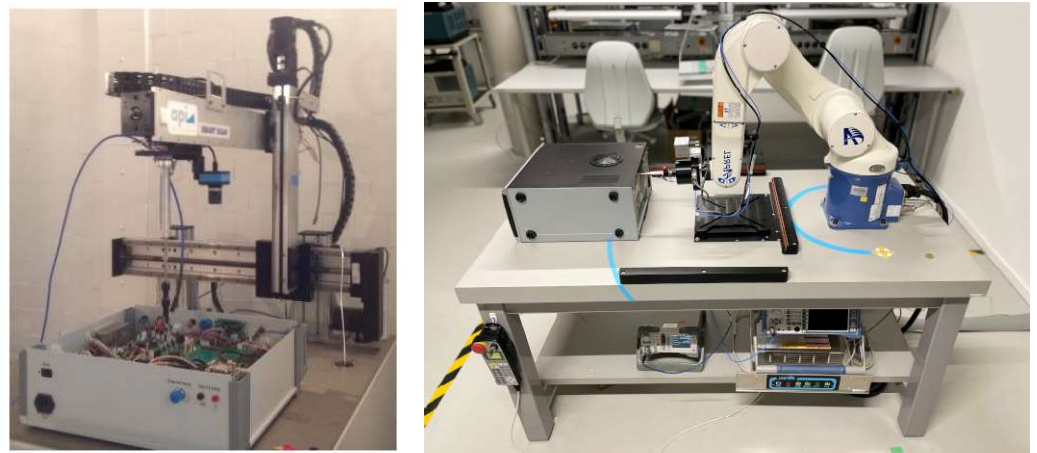


Figure 1. 3D Scanner equipment by two different suppliers.

2.1. General Equipment Overview and Antenna Specifications

The scanner has been developed from existing laser engraver equipment, whose components have been repurposed as follows. The aluminum chassis has been used as the main mechanical support, while the plexiglass parts have been used to complete the aluminum structure, including the legs. The stepper motors are two motors used for movement along the x - and y -axis. The main control board hosts the stepper motors' driver boards and connectors. Toothed belts and wheels have been used for the movement transmission together with motors. Finally, the power adapter has been used to generate 12 V DC from the mains. The laser unit has been not repurposed because it is not useful for the scanner. Similarly, the Arduino Nano board has been not repurposed because its firmware was programmed for laser printing purposes only and was not designed to be controlled by custom software.

A nylon 3D-printed head holding the antennas in the desired positions has substituted the laser (Figure 2). So, the customized firmware has been properly written in the EEPROM of a new Arduino Nano board to maintain the same pinout and the native connectors.

The test equipment used is listed below:

- ESRP7 Rohde & Schwarz Emi test receiver
- GPIB—USB—HS National Instruments GPIB to USB converter
- TDK-Lambda power supply
- Beehive Electronics near-field probes

The adopted Beehive Electronics near-field probes are commercial antennas specifically designed to detect proximity electric and magnetic fields. They are cheap detectors, adapted to an impedance of 50Ω . A stub antenna (diameter of head 0.08 inches), suitable to measure the electric field, and three different sizes of loop antennas appropriate to measure the magnetic field have been used. The smallest size allows the best spatial resolution and has a diameter of 0.25 inches. In Figure 2, the antennas and the nylon head of the machine with a mounted antenna are shown.

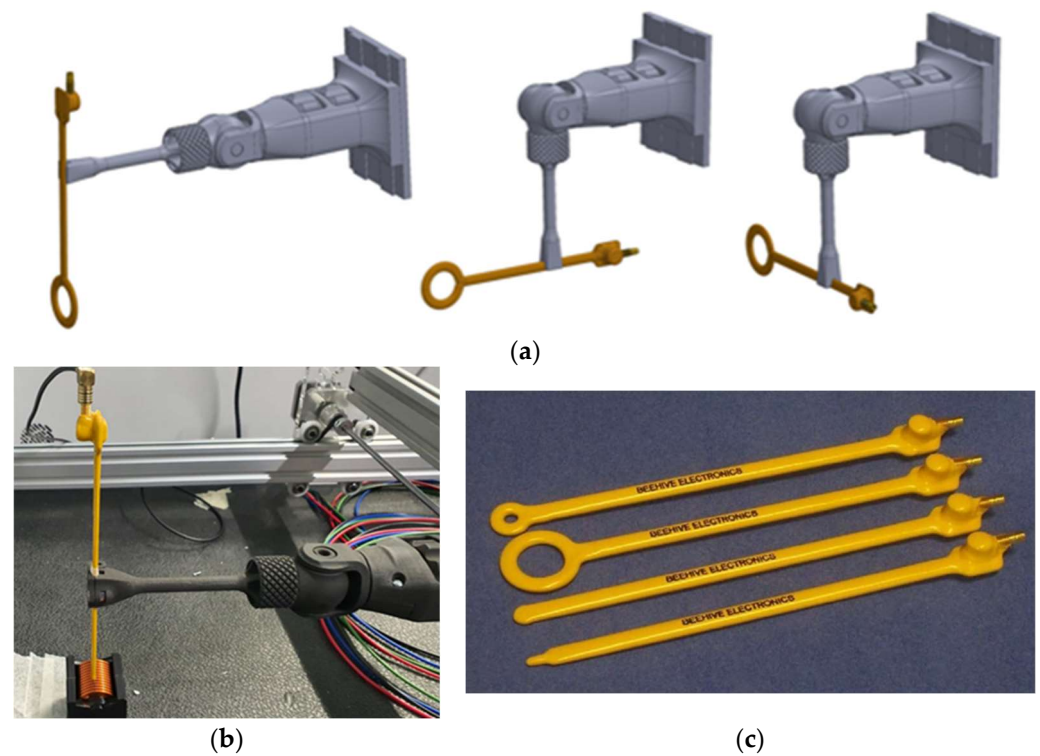


Figure 2. Scanner head (a) designed movements; (b) 3D-printed tool) and (c) antennas.

Figure 3 illustrates the conversion curves to compute the E field in V/m and the B field in T starting from the spectrum acquired in dBm with an EMI test receiver or a spectrum analyzer. In the datasheet [13], besides the curves, the formulas needed to convert the dBm measured by the spectrum analyzer into T or V/m, and taking into account the frequency dependence, are given as:

$$E_{\left(\frac{V}{m}\right)} = 10^{\frac{P_{out}(dBm) + 113.2 - 20 \log_{10}(F(MHz))}{20}} \quad (1)$$

$$B_{(T)} = 10^{\frac{P_{out}(dBm) - X - 20 \log_{10}(F(MHz))}{20}} \quad (2)$$

where X is a number whose value is reported in Table 1.

The equipment can execute a full scan on an XY plane once the desired distance of Z0 between the board and the antenna in the direction of the z-axis has been fixed. The developed scanner has been customized for the automatic scanning of a rectangular area at a preselected height (Z0) from the board. However, the lack of z-axis handling is not a limitation for the considered application. Finally, the minimum Z0 is bounded by the highest board component because the aim is field measurement in a rectangular area; thus, it is unnecessary for any stepper motor to height change during the measurements.

Table 1. X factor in Equations (1) and (2) for each antenna.

Antenna Type	X	3 dB Frequency (MHz)	First Resonance (MHz)
100C (large loop)	85.1	50	500
100A (medium loop)	65.2	1000	2600
100B (small loop)	42.2	3100	>6000

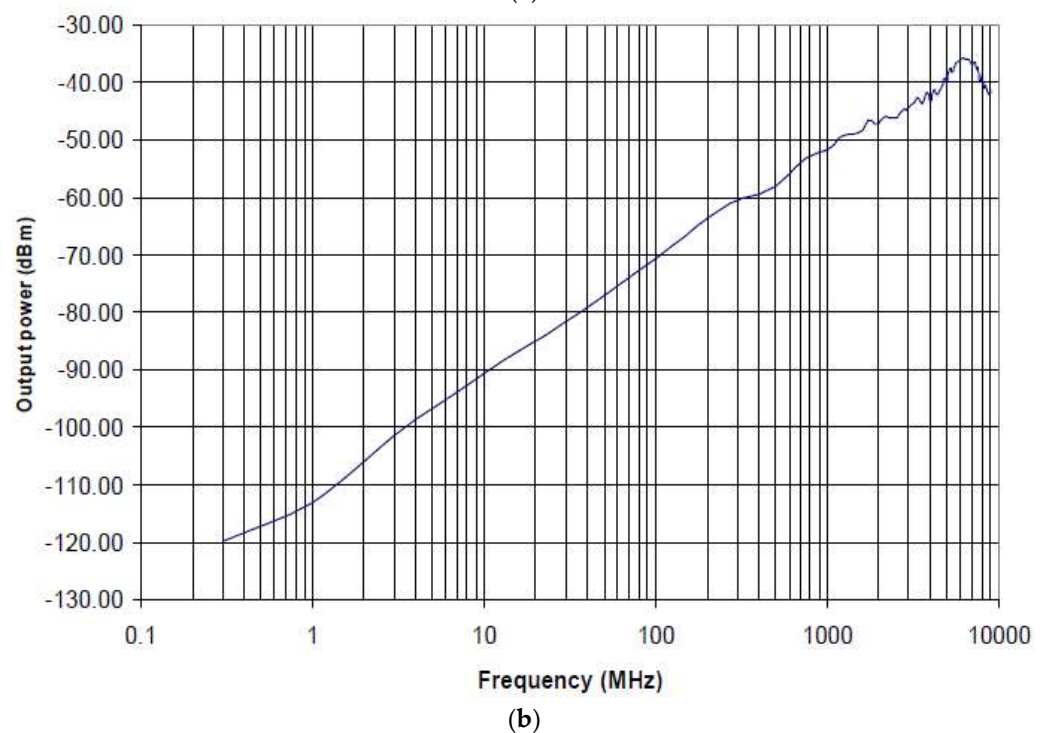
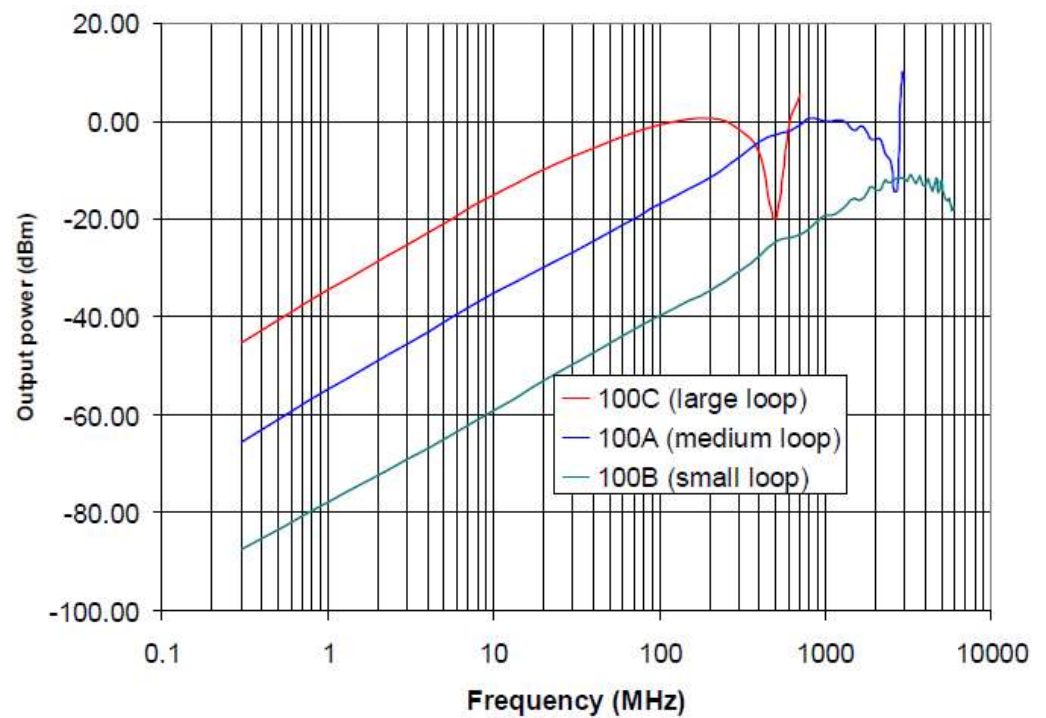
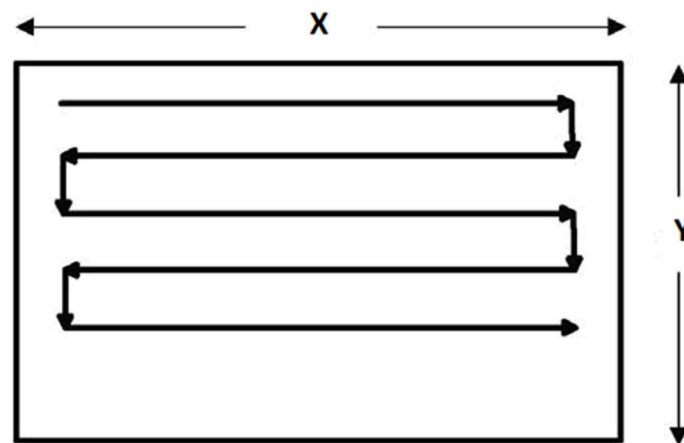
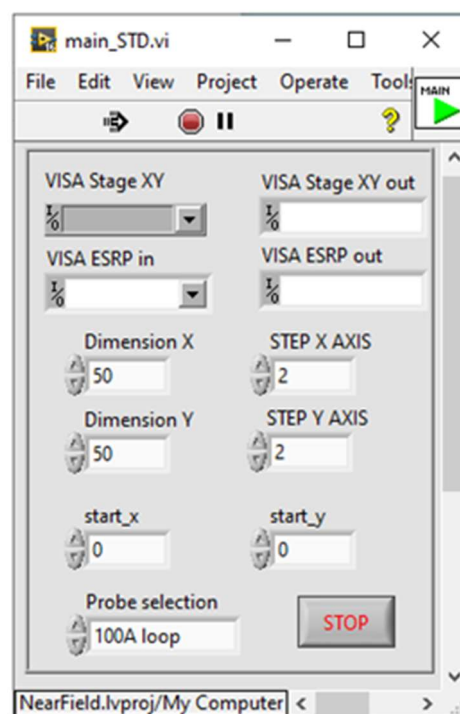


Figure 3. Antenna conversion curves: (a) output power vs. frequency at $1 \mu\text{T}$ field strength; (b) output power vs. frequency at 1 V/m field strength.

Distance Z_0 is the center of the loop for the magnetic field measurements and the bottom edge for the electric field measurements. Starting from an initial point (X_0, Y_0, Z_0) , two stepper motors move the antenna along a preset path parallel to the board surface, as shown in Figure 4a, thus covering an area equal to a rectangle of width X and height Y . Figure 4b shows a picture of the LABVIEW software (2016) interface, which manages the scanning process. This LABVIEW scanning window assigns the dimensions of the scanning area, the scanning step, the starting position and the type of antenna.



(a)



(b)

Figure 4. Pattern of the scanning path (a) and LABVIEW control panel for the scanning process (b).

Then, for each position of the antenna along the path, the LABVIEW software acquires a full spectrum of the signal (Figure 5) in the chosen frequency band by means of an EMI test receiver or a spectrum analyzer.

The acquisition is fully automatic and managed by the software. The LABVIEW software communicates with the machine controller as if it were a VISA (Virtual Instrument Software Architecture) instrument; the Arduino Nano board is already equipped with a USB to UART (serial) converter, which allows the PC to communicate directly with the on-board Atmel microcontroller. A list of simple commands has been defined to request information from the board about the head position, moving the head of a specific step and setting some tuning parameters. For example, some commands are needed to tune the size of the step, both in the X and Y directions. Since the head is not equipped with position encoders, the microcontroller saves the position of the head into its EEPROM (electrically erasable programmable memory) every twenty seconds.

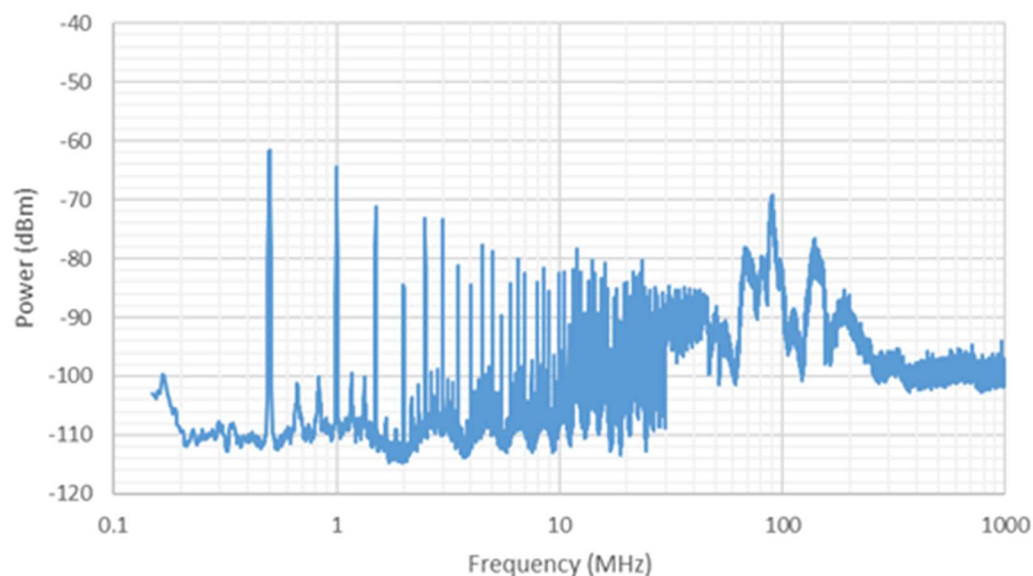


Figure 5. Example of spectrum acquired at a point in the scanned pattern grid.

To avoid damaging the EEPROM (which has a limited number of writing repetitions) in a short time, the firmware uses a smart algorithm that is able to write a location only if the byte to be written is different from the one already stored there, and it is also able to use a pointer in order to write cyclically in the whole memory and not in the same locations all the time. The firmware communicates with the PC when a requested operation is concluded and a new one can be executed; this is useful to synchronize the LABVIEW and the firmware operations. In Figure 6a, a full image of the scanning equipment is shown.

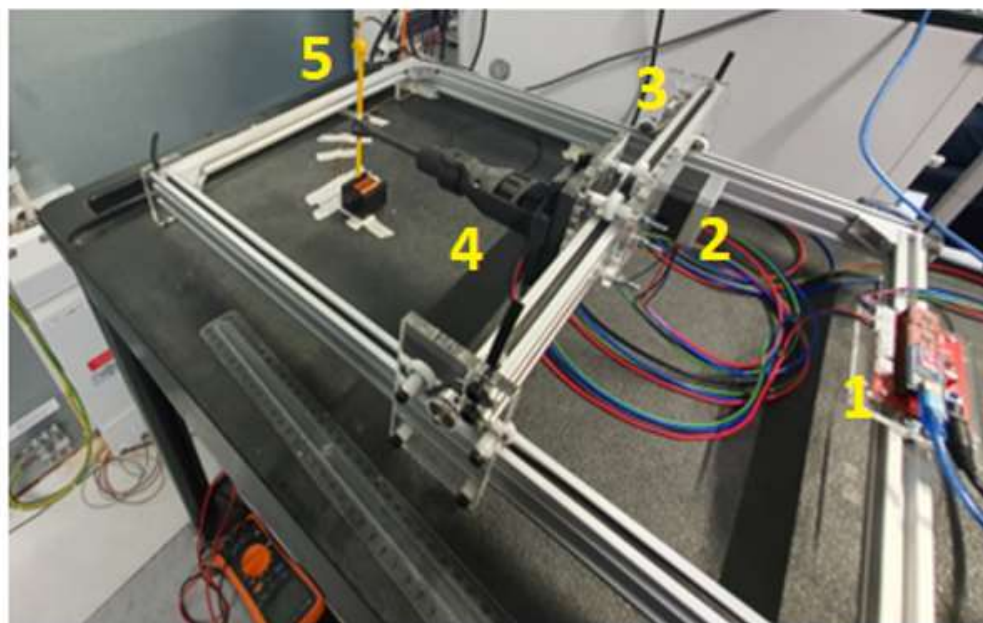
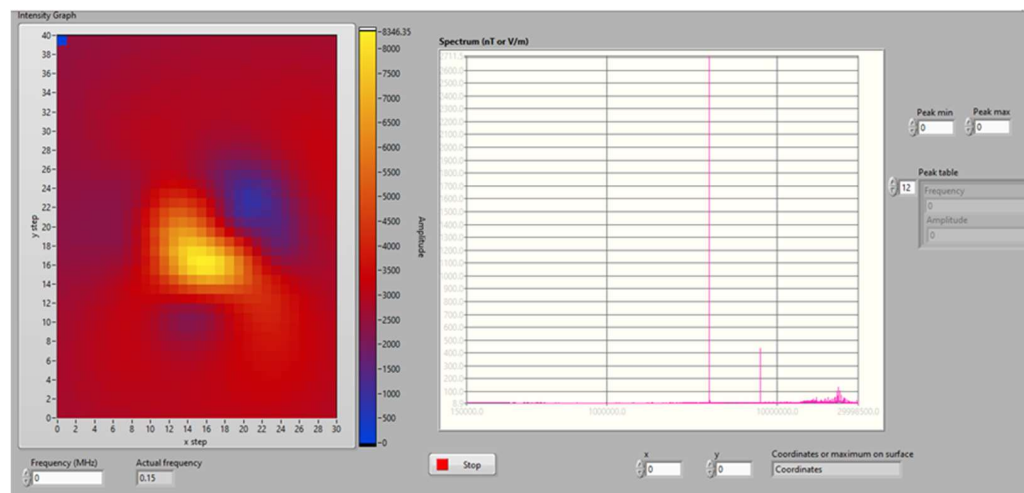


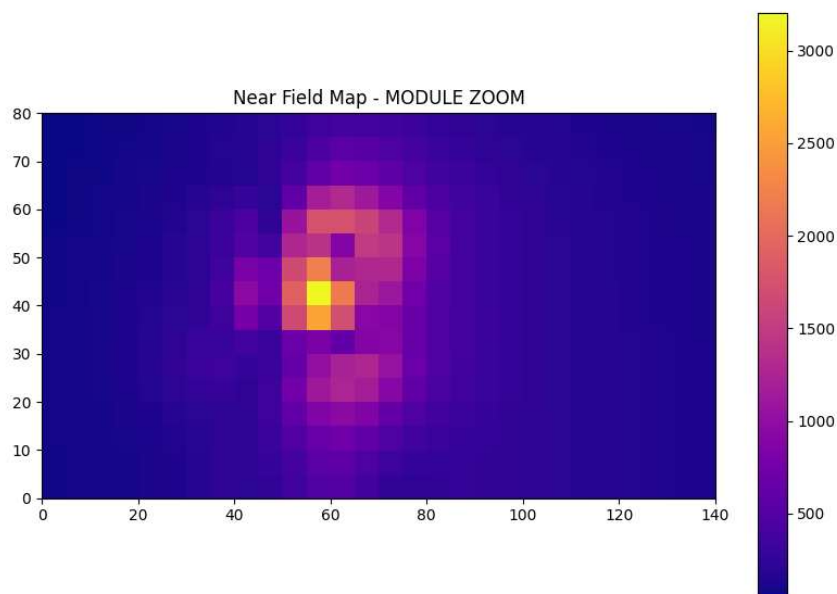
Figure 6. Equipment overview: 1—microcontroller Arduino Nano board and A4988 stepper motor drivers; 2—stepper motor for Y direction; 3—stepper motor for X direction; 4—nylon 3D printed head; 5—magnetic field antenna.

The spectrum and coordinates are saved for post-processing purposes for each point of the scanned surface. For example, using a color map to show the field intensity or one of their components, it is possible to also show the map of a single component of B or E magnitude on an XY plane. In the same post-processing window, it is possible to see the

spectrum of the fields or that of its components. In this regard, portable Python 3 software has also been developed; this can be distributed together with the data files generated by the EMI receiver and allows the easy exploration of the fields' maps for each orientation and each frequency (Figure 7).



(a)



(b)

Figure 7. Near-field map. (a) LABVIEW post-processing view, (b) Python 3 post-processing software results.

Obviously, the proposed scanner is not conceived for applications where more accurate and extensive analyses have to be performed, especially for certification purposes. As mentioned before, the proposed solution enables the performance of a rough measurement of electromagnetic emissions in all the cases where, usually, no measurements are performed due to the lack of an expensive scanner. Therefore, although the accuracy is probably below that of commercial scanners, a rough comparison among different board solutions can be performed in these cases. Moreover, the accuracy depends on different factors, especially the accuracy of the antennas, which is often not declared in the datasheet (as the ones used in the case study of this work).

The spatial resolution depends on the minimum movement possible along the x- and y-axis of the chassis and the antenna dimension. For example, the minimum step is 1 mm with 100 B and 100 D antennas. Finally, a sampling rate of one step per second has been measured when the frequency is in the interval [1 MHz–1 GHz].

2.2. Controller Board Description

The controller board is made with an Arduino Nano microcontroller. The Arduino drives the two A4988 cheap stepper motor controllers through two pins. One sets the direction by pulling the DIR inputs of the A4988 boards up to 3.3 V or pulling them down to 0, and the other sends a square wave to the STEP pins (one period for one step). The microcontroller board also pulls down the ENABLE input in order to switch ON or OFF the modules. In Figure 8a, a simplified schematic of the controller is shown, while in Figure 9, the A4988 driver photo and pinout are shown.

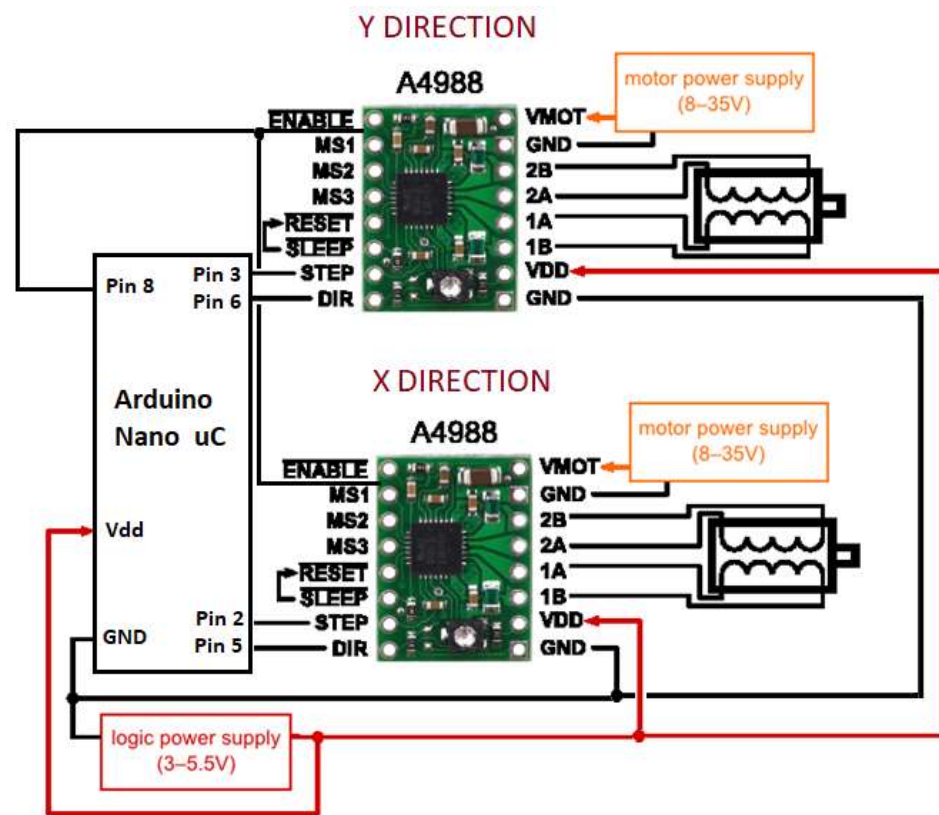


Figure 8. Simplified controller schematic.

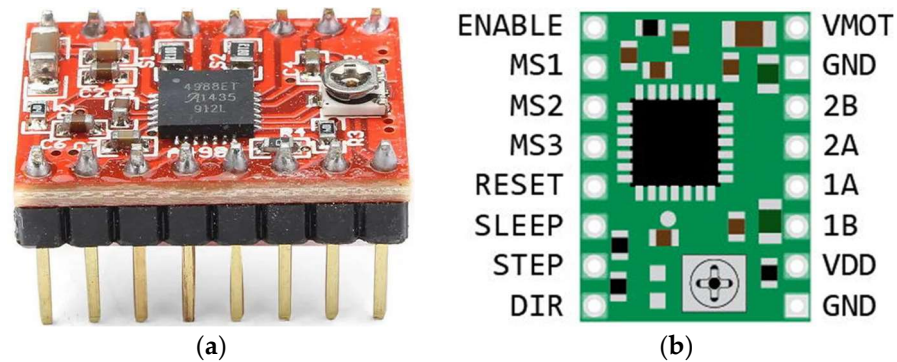


Figure 9. A4988, stepper motor controller: (a) driver photo and (b) its pinout.

The microcontroller and the logical circuitry of the A4988 boards are supplied by USB. The power circuitry of each A4988 board is instead supplied by an external power supply adapter.

The pins that drive the stepper motor are 1A 1B and 2A 2B. The motor supply is connected to the pin VMOT and its closest GND. The pins SLEEP and RESET are generally connected together. MS1, MS2 and MS3 are digital inputs used to tune the micro-step resolution (Table 2).

Table 2. Micro stepping resolution truth table.

MS1	MS2	MS3	Resolution	Excitation Mode
L	L	L	Full step	2 Phase
H	L	L	Half step	1–2 Phase
L	H	L	Quarter step	W1–2 Phase
H	H	L	Eighth step	2W1–2 Phase
H	H	H	Sixteenth step	4W1–2 Phase

The typical signal that drives the module and the corresponding current on the motors is shown in Figure 10.

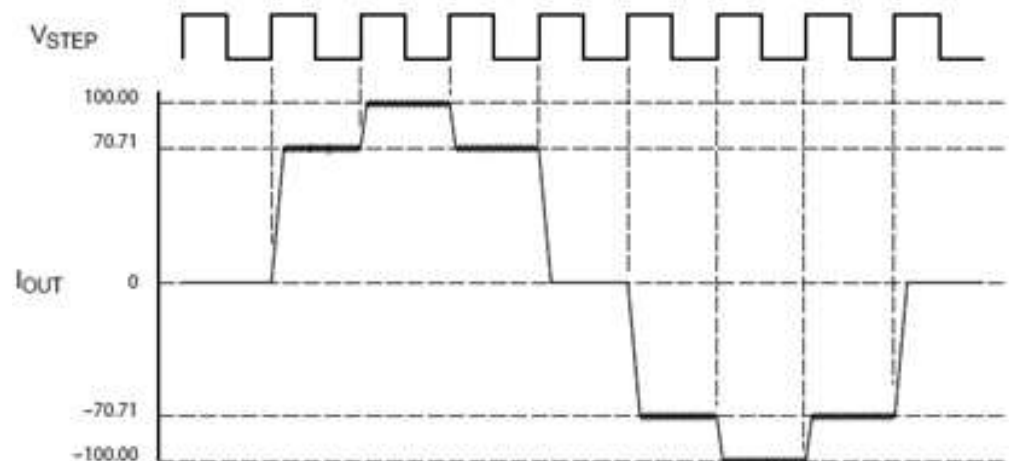


Figure 10. Typical signal on stepper motors.

2.3. Equipment Firmware Description

The conceived method for developing the firmware is an original contribution because it enables the equipment control from software that is different from those used in this work. More specifically, the firmware has been structured as a command-based firmware for machine control similar to commercial equipment, but, in contrast, it enables the control of the scanner using software different from the one developed in LABVIEW for this work.

A list of commands to set some tuning parameters and manage the head's movement has been defined. For some commands, the related queries have been defined to obtain the value for that parameter instead of setting it. Table 3 shows a complete list of commands and their descriptions.

Each command returns the information related to the end of its execution, which is useful for synchronizing the firmware with LABVIEW software. Hence, LABVIEW routines wait for an answer from the microcontroller before executing the next scheduled operation.

Some tuning parameters that are not present in the original firmware and are useful to increase accuracy have been introduced in the developed firmware. In detail, they enable the setting of the stepper motor movements before the first use of the equipment and during the calibration. In addition, the steps along the x - and y -axis can be set separately, thus improving the functionality of the equipment.

Table 3. Equipment virtual Com port commands.

Command	{dir}	{Query}	{Value}	Short Description
STEP_SIZE_{dir}<space>{value} STEP_SIZE_{query}	X, Y	X?, Y?	nnn	Size of single step setting/query
MOV_{dir}<space>{value}	X, Y, 0	No query	+nnn, -nnn	Move to set position, "+" forward, "-" back, "0" to the axis origin
DELAY_{dir}<space>{value} DELAY_{query}	X, Y	X?, Y?	nnn	Set the speed of movement
TRIM_XY<space>{value} TRIM_XY{query}	No dir	?	nnn	Set a multiplication factor to adjust stem size
MAX_{dir}<space>{value} MAX_{query}	X, Y	X?, Y?	nnn	Set maximum steps for each direction
POS_{query}	No dir	X?, Y?		Ask for position as number of steps

A serious challenge has been the lack of position encoders and limit switches, which involve potential damage to the motors and transmission belts. The developed firmware pre-sets the maximum x and y positions and stores the current position of the scanning head in the EEPROM to solve this problem. The optimal management of EEPROM writings has been another challenge because the microcontroller's lifetime reduces with increasing writing numbers. A smart save/retrieve algorithm has been developed to face this issue. Considering an EEPROM size of 1024 bytes, the first 21 bytes are reserved for quantities that change infrequently, such as the step size and maximum X and Y. The position of the scanning head, instead, is stored every 20 s, starting from byte 22 of the EEPROM. Each time the position has to be written, a pointer "*" is moved forward of 8 bytes, and then six bytes are saved: three encode the X position and three encode the Y position. In this way, the firmware can know the current position of the pointer by reading the EEPROM interval 22-1024. Once the pointer is found, it knows that the six bytes that follow contain the XY position of the head. To avoid unnecessary operations, the firmware checks the value of a byte in the EEPROM before writing the new one. When it is equal to the old one, the firmware avoids writing it; otherwise, it writes the new value.

2.4. Equipment LABVIEW Software Description

Figure 11 shows the developed LABVIEW main panel, in which some general parameters can be assigned. In detail, they are:

- the VISA address of the ESRP7 EMI test receiver;
- the COM port of the Arduino Nano controller of the position equipment;
- the X and Y dimensions of the scanning area;
- the minimum step along the X and Y directions.

In the same panel, three switches allow, respectively, the scanning of the module, the post-processing of the module measurements, to move the head to a specified position (e.g., the starting point for the scanning process). The panel enables the selection of the type of antenna that, in turn, determines the conversion formula that will be used to transform the field measurements according to Equations (1) and (2).

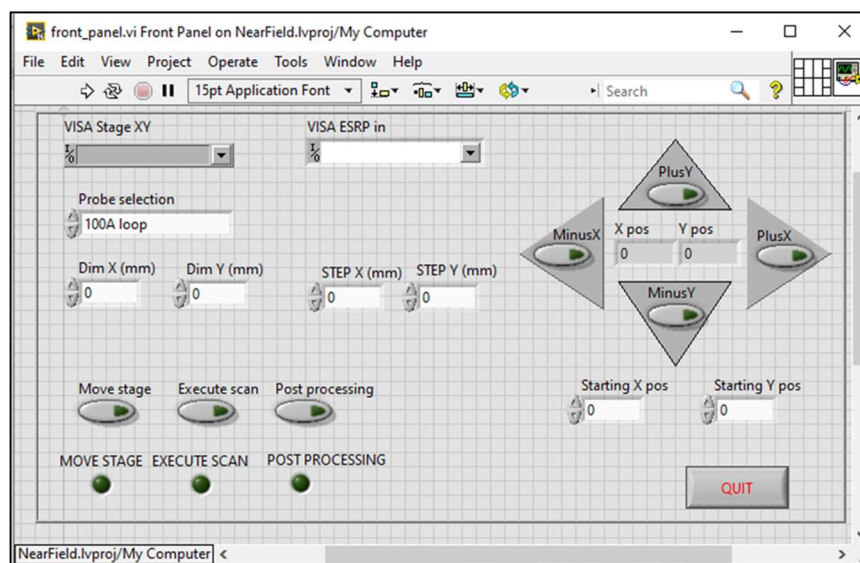


Figure 11. LABVIEW control software main panel.

The panel routine waits in the IDLE state, which is repeated until the STOP command is selected or any other choice is taken. A complex flow is executed if the command button named “Move stage” is selected. More specifically, if a specific position is specified with X, Y or both values are higher than zero, the head moves to these XY coordinates. Otherwise, it moves itself according to the value reached by pressing one of the arrow commands. The process also checks if the X and Y coordinates exceed the maximum values or are negative and, in that case, corrects them. When the scanning routine is started by the front panel, this moves the head to the (0, 0) position and then to the position (X0, Y0) chosen as the starting point for the scanning process. Then, the software also asks the microcontroller to know the max X and Y values stored in its EEPROM. They are the maximum allowed values that can be chosen to avoid the stepper motors forcing the head to move too close to the edges of the system. The total number of steps is also computed before entering the main scanning cycle. First, the head is moved along the X direction of one step, starting from the X0 position, until the maximum value ‘max X’ is reached. Then, a step along the Y position is performed, and the head starts to move along the X direction again but in the opposite way until the position X0 is reached. A new Y step is performed, and so on, in accordance with Figure 4a. The scanning operation continues cyclically until the max X and max Y positions are reached. At each point, the complete spectrum is measured by the ESRP7. Once the acquisition is performed, the next step is executed. At the end, the spectrum converted into values of field intensity is stored in a matrix, with one column for each pixel in the scanned surface. When the scanning process is finished, the matrix hosting all the measured values of the field and the coordinates of each point on the scanned surface is saved into a file for post-processing purposes.

Figure 12 shows a flowchart with more information about the data acquisition algorithm. Concerning the data processing, a conversion routine has been embedded in the post-processing software used to relate the field magnitude with colors. A post-processing LABVIEW routine containing some automatic analysis capabilities has also been developed. In particular, it shows the maximum magnitude of the fields for each frequency of the analyzed spectrum. Moreover, the map for the frequency where higher fields (B or E) have been found can be requested. The developed Python post-processing software automatically provides the field intensity by positioning the pointer at the desired X–Y map pixel. The possibility to separately show the three components of the B or E fields and the map magnification are additional features.

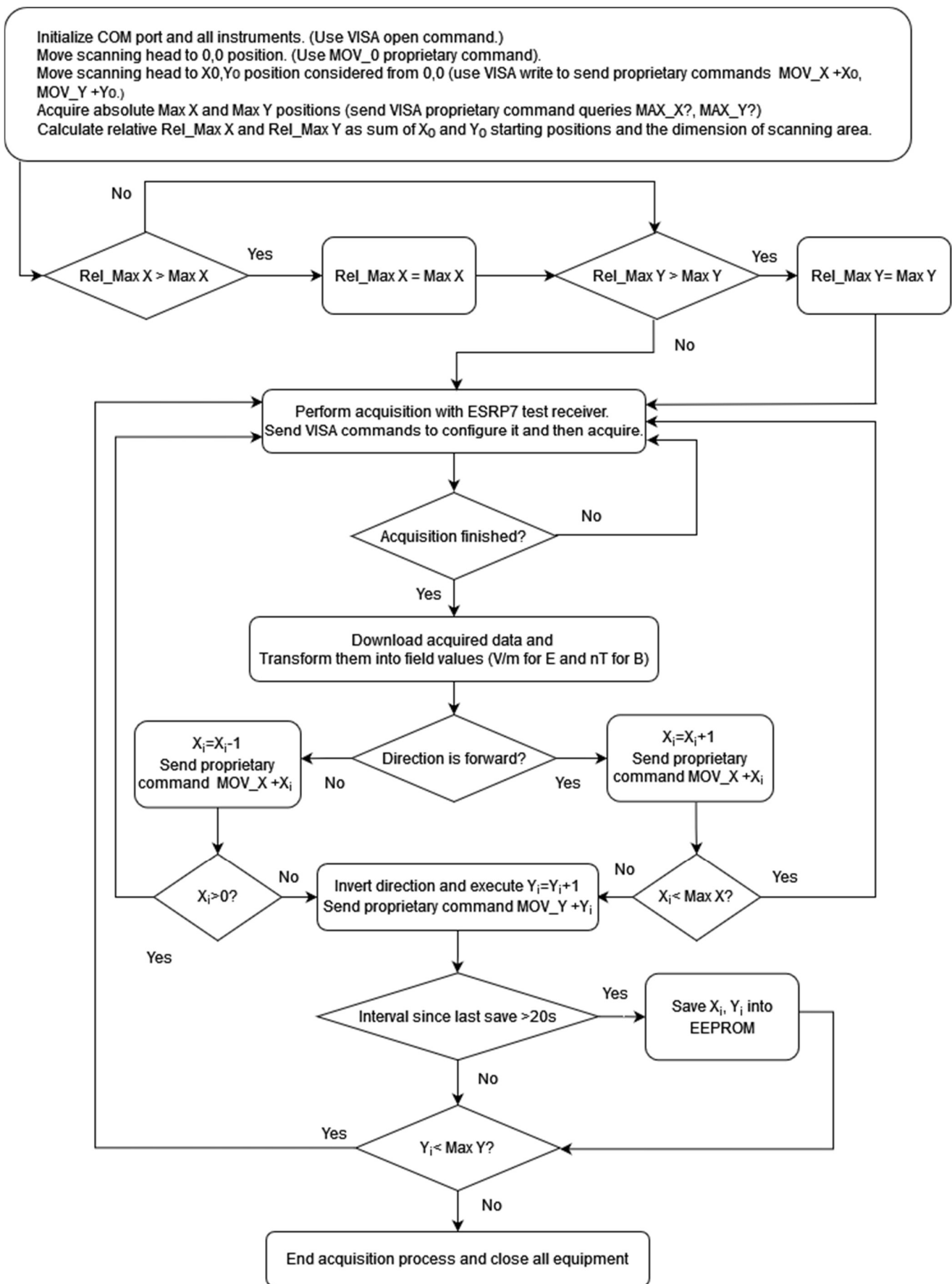


Figure 12. Data acquisition algorithm.

3. A Case Study: Bi-Directional GaN DC/DC Converter

The gallium nitride transistor market is increasing due to the advantages in terms of efficiency and power density [14]. These good features are enabled by their high switching speed (a few nanoseconds) [15,16]. On the other hand, extremely high dv/dt (over 100 V/ns) of the associated voltage waveforms induce severe electromagnetic interference [17–20]. Hence, the proposed inexpensive system for automatic near-field scanning has been used to analyze the electromagnetic noise generated by the output inductor in a GaN-based bi-directional DC/DC switching converter board. The converter has been used in the 48V–12V step-down buck configuration; a simplified schematic is shown in Figure 13.

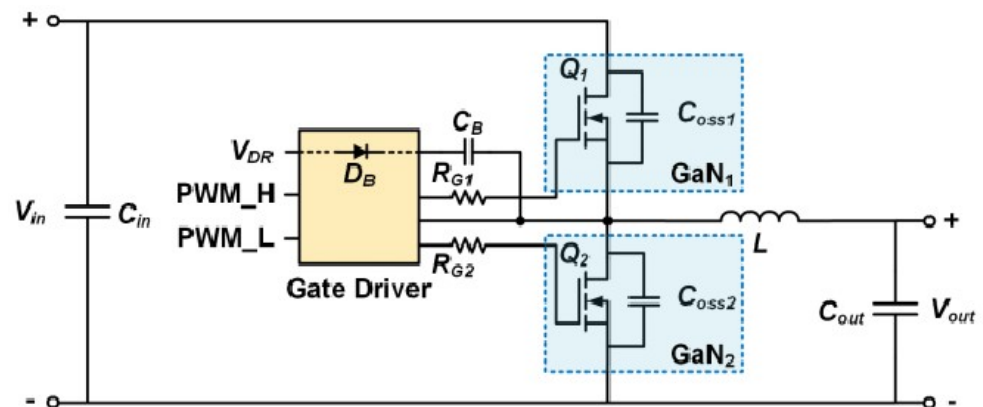


Figure 13. Schematic of a generic GaN buck DC–DC converter.

A picture of a board where the scanning process has been executed is provided in Figure 14. The application is managed by a driver controller that is connected, through resistors, to the GaN half-bridge integrated power stage and the output LC filter.

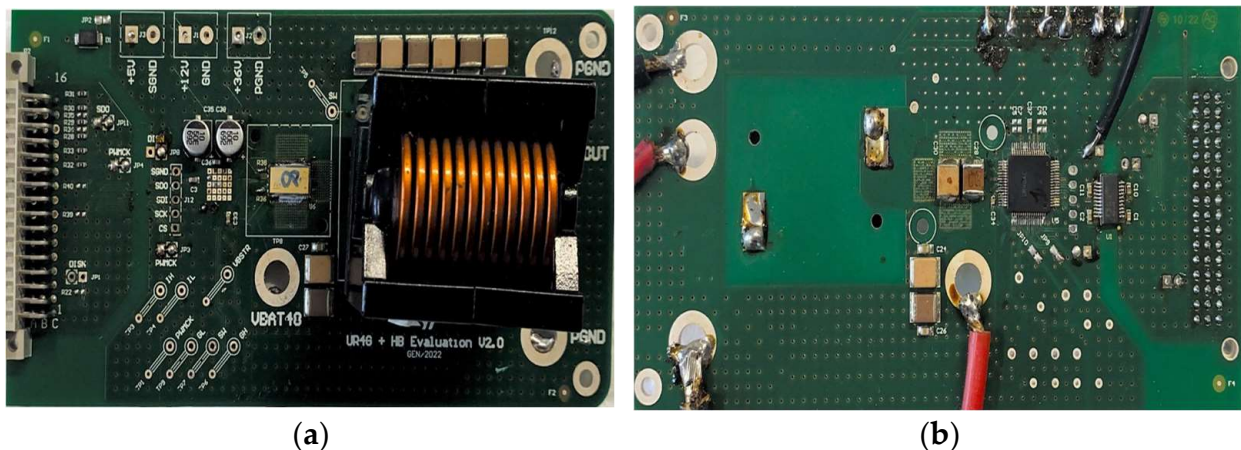


Figure 14. Board of the GaN buck DC–DC converter: (a) front view, (b) rear view.

For this device, when working in the synchronous buck mode, oscillations (Figure 15) of the switch node caused by parasitic inductances and fast commutations were observed. The ringing generates an electromagnetic field and, therefore, problems of electromagnetic noise. However, to test the scanning equipment, only magnetic induction B above the big filtering output circuit inductor has been mapped.

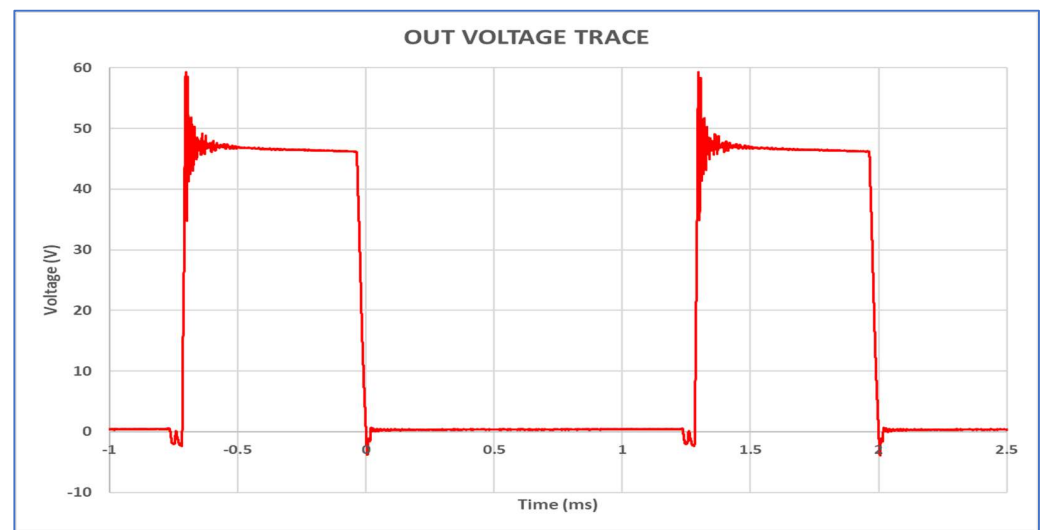


Figure 15. Switching node voltage.

A scan along each axis has been performed in order to obtain the three components of magnetic induction B (Figure 16). The antenna with the smallest loop (type 100B, Table 1) has been used. For each scanned surface unit, the EMI test receiver measured and stored the emissions in a range of frequencies from 150 kHz to 1 GHz.

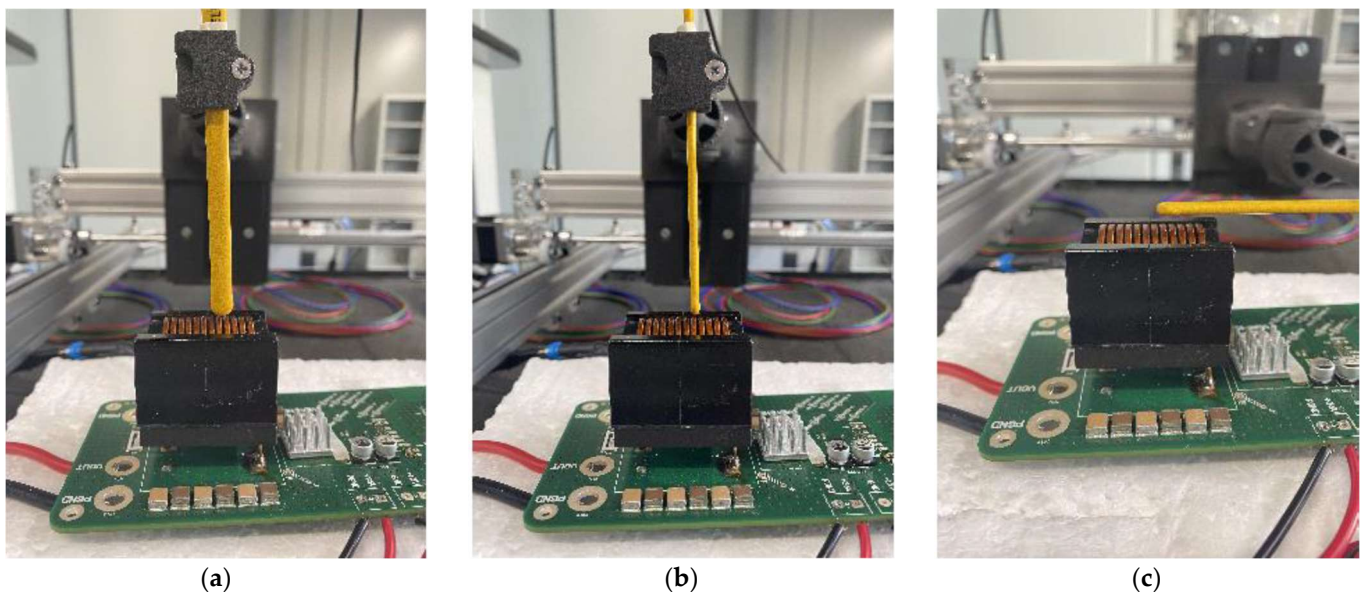


Figure 16. View of magnetic field acquisition along (a) x direction, (b) y direction and (c) z direction.

By means of the post-processing software, the image of the magnitude of the magnetic field was obtained. Once the colored image of the B magnitude on an XY plane (at a given distance from the scanned element) has been created, it is possible to set an opportune level of transparency and superimpose this image on the real image of the part of the board scanned. The maximum magnitude of the magnetic field at the converter frequency (500 kHz) was $3.83 \mu\text{T}$, and it was located almost in the center of the inductor. The minimum, located at the scanning area edge, was about 300 nT. In the inductor area, the average field was about $2.5 \mu\text{T}$. At 30–40 MHz, the magnetic field was mainly concentrated on the exposed ferrite parallel parts (left and right sides of the coil). The maximum magnitude of the magnetic field was about $300 \mu\text{T}$. In the range 140–150 MHz, a very uniform B distribution was observed. Figure 17 shows a map of the magnetic field magnitude at 500 kHz.

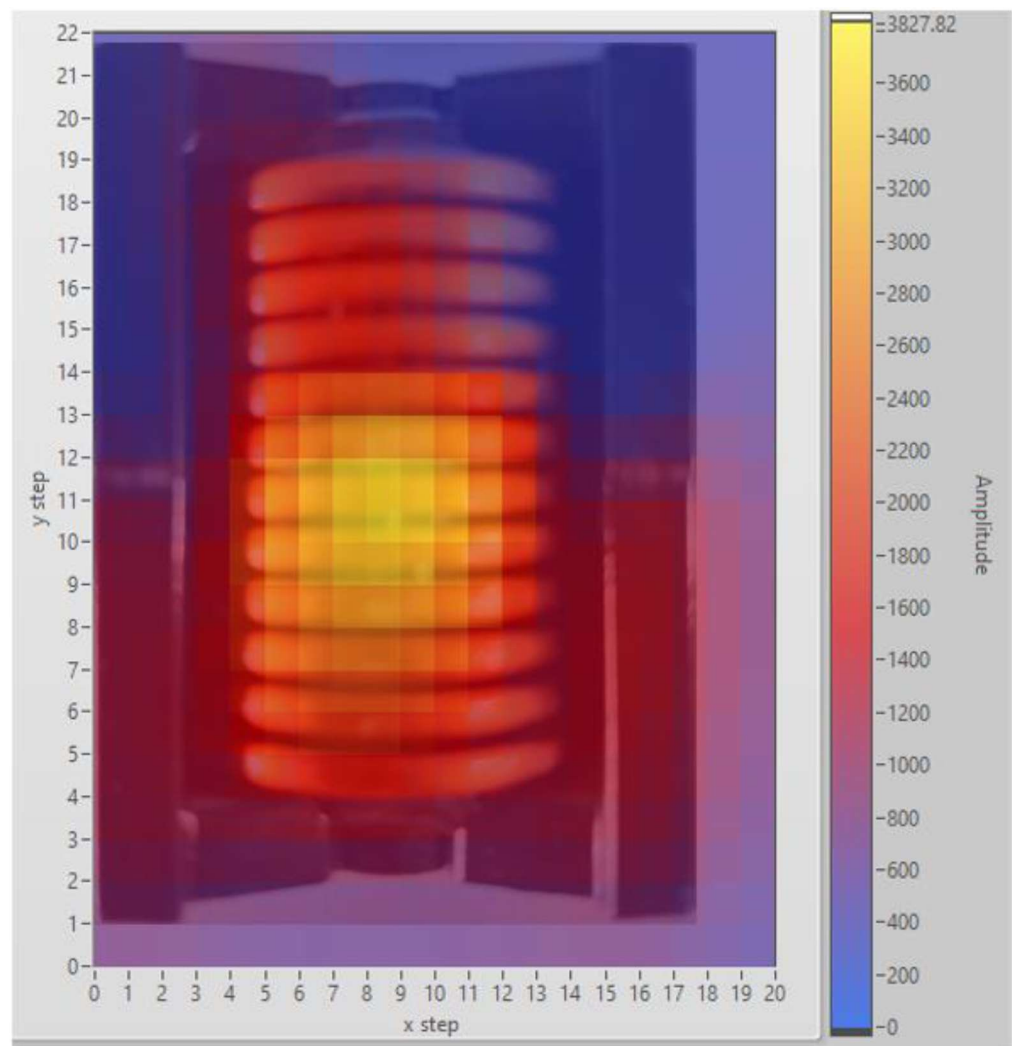


Figure 17. B magnitude detected on the output filter inductor of the bi-directional GaN DC/DC buck converter.

4. Conclusions

The near-field scanner described in this document is an inexpensive system that is able to map the spatial distribution of electric and magnetic fields. Thanks to the head, which is specifically designed for the purpose, it is possible to set distances ranging from a few millimeters up to several centimeters. The resolution along the X and Y directions is accurate enough to guarantee very defined maps of the electromagnetic field over a PCB. The vertical distance of the head from the board is limited only by the higher component in the board itself. The application to different boards and comparing the scanner measurements with the simulation of benchmarks are potential future developments of this activity.

The map acquired allows for an understanding of where the highest emissions on the board surface are located and finding the components and/or traces that generate them, thus allowing the optimization of its layout. The cost of the developed system is less than two thousand dollars, thus making it useful in any application where an investment in expensive commercial equipment is not justified.

Author Contributions: Conceptualization, N.S.; Methodology, S.A.R.; Investigation, S.G. and S.B.; Resources, S.G.; Data curation, S.B.; Writing—original draft, S.G. and S.A.R.; Writing—review & editing, N.S.; Supervision, S.A.R.; Funding acquisition, S.G. All authors have read and agreed to the published version of the manuscript.

Funding: This research received no external funding.

Data Availability Statement: Data are contained within the article.

Conflicts of Interest: The authors declare no conflict of interest.

References

1. Aswin, A.M.; Sundar, S. Electromagnetic Interference (EMI) and Electromagnetic Compatibility (EMC) in Real Time Applications—Survey. *Int. J. Mech. Eng. Technol.* **2018**, *9*, 474–482.
2. Electromagnetic Compatibility (EMC) Directive. Available online: https://single-market-economy.ec.europa.eu/sectors/electrical-and-electronic-engineering-industries-eei/electromagnetic-compatibility-emc-directive_en (accessed on 23 September 2023).
3. Paul, C.R. *Introduction to Electromagnetic Compatibility*, 2nd ed.; Wiley-Interscience: Hoboken, NJ, USA, 2006.
4. Li, C.; Ma, Q.; Tong, Y.; Wang, J.; Xu, P. A survey of conductive and radiated EMI reduction techniques in power electronics converters across wide-bandgap devices. *IET Power Electron.* **2023**, *16*, 2121–2137. [[CrossRef](#)]
5. Minardi, G.; Greco, G.; Vinci, G.; Rizzo, S.A.; Salerno, N.; Sorbello, G. Electromagnetic Simulation Flow for Integrated Power Electronics Modules. *Electronics* **2022**, *11*, 2498. [[CrossRef](#)]
6. Wunsch, B.; Skibin, S.; Forsström, V.; Stevanovic, I. EMC Component Modeling and System-Level Simulations of Power Converters: AC Motor Drives. *Energies* **2021**, *14*, 1568. [[CrossRef](#)]
7. Radchenko, A.; Khilkevich, V.; Bondarenko, N.; Pommerenke, D.; Gonser, M.; Hansen, J.; Keller, C. Transfer function method for predicting the emissions in a -cisp25 test-setup. *IEEE Trans. Electromagn. Compat.* **2014**, *56*, 894–902. [[CrossRef](#)]
8. Mariscotti, A.; Ogunsola, A.; Sandrolini, L. Survey of models and reference data for prediction of e.m. field emissions from electrical machinery. In Proceedings of 8th IEEE Symposium on Diagnostics for Electrical Machines, Power Electronics & Drives (DEMPED), Bologna, Italy, 5–8 September 2011. [[CrossRef](#)]
9. Rajagopal, N.; DiMarino, C.; DeBoi, B.; Lemmon, A.; Brovont, A. EMI Evaluation of a SiC MOSFET Module with Organic DBC Substrate. In Proceedings of the IEEE Applied Power Electronics Conference and Exposition (APEC), Phoenix, AZ, USA, 14–17 June 2021; IEEE: Piscataway, NJ, USA, 2021.
10. Chen, H.; Liu, Q.; Li, Y.; Huang, C.; Zhang, H.; Xu, Y. Research on the Method of Near-Field Measurement and Modeling of Powerful Electromagnetic Equipment Radiation Based on Field Distribution Characteristics. *Energies* **2023**, *16*, 2005. [[CrossRef](#)]
11. Zhang, B.; Wang, S. A Survey of EMI Research in Power Electronics Systems With Wide-Bandgap Semiconductor Devices. *IEEE J. Emerg. Sel. Top. Power Electron.* **2020**, *8*, 626–643. [[CrossRef](#)]
12. Chen, H.; Wang, T.; Feng, L.; Chen, G. Determining Far-Field EMI From Near-Field Coupling of a Power Converter. *IEEE Trans. Power Electron.* **2014**, *29*, 5257–5264. [[CrossRef](#)]
13. Beehive ELECTRONICS 100 Series EMC Probes Datasheet. Available online: <https://beehive-electronics.com/datasheets/100SeriesDatasheetCurrent.pdf> (accessed on 23 November 2023).
14. Scrimizzi, F.; Cammarata, F.; D’Agata, G.; Nicolosi, G.; Musumeci, S.; Rizzo, S.A. The GaN Breakthrough for Sustainable and Cost-Effective Mobility Electrification and Digitalization. *Electronics* **2023**, *12*, 1436. [[CrossRef](#)]
15. Letellier, A.; Dubois, M.R.; Trovao, J.P.; Maher, H. Gallium Nitride Semiconductors in Power Electronics for Electric Vehicles: Advantages and Challenges. In Proceedings of the 2015 IEEE Vehicle Power and Propulsion Conference (VPPC), Montreal, QC, Canada, 19–22 October 2015.
16. Musumeci, S.; Mandrile, F.; Barba, V.; Palma, M. Low-Voltage GaN FETs in Motor Control Application; Issues and Advantages: A Review. *Energies* **2021**, *14*, 6378. [[CrossRef](#)]
17. Derkacz, P.B.; Schanen, J.-L.; Jeannin, P.-O.; Chrzan, P.J.; Musznicki, P.; Petit, M. EMI Mitigation of GaN Power Inverter Leg by Local Shielding Techniques. *IEEE Trans. Power Electron.* **2022**, *37*, 11996–12004. [[CrossRef](#)]
18. Rajeswari, P.; Manikandan, V. Analysis of effects of MOSFET parasitic capacitance on non-synchronous buck converter electromagnetic emission. *Ain Shams Eng. J.* **2023**, *14*. [[CrossRef](#)]
19. Raciti, A.; Chimento, F.; Musumeci, S.; Privitera, G. A New Thermal Model for Power Mosfet Devices Accounting for the Behavior in Unclamped Inductive Switching. *Microelectron. Reliab.* **2016**, *58*, 3–11. [[CrossRef](#)]
20. Middelstaedt, L.; Strauss, B.; Lindemann, A. Analyzing EMI issues in a DC/DC converter using GaN instead of Si power transistors. In Proceedings of the 2019 10th International Conference on Power Electronics and ECCE Asia (ICPE 2019-ECCE Asia), Busan, Republic of Korea, 27–30 May 2019.

Disclaimer/Publisher’s Note: The statements, opinions and data contained in all publications are solely those of the individual author(s) and contributor(s) and not of MDPI and/or the editor(s). MDPI and/or the editor(s) disclaim responsibility for any injury to people or property resulting from any ideas, methods, instructions or products referred to in the content.